

Andreev bound states and π -junction transition in a superconductor / quantum-dot / superconductor system

Yu Zhu, Qing-feng Sun and Tsung-han Lin*

State Key Laboratory for Mesoscopic Physics and

Department of Physics, Peking University, Beijing

100871, China

()

Abstract

We study Andreev bound states and π -junction transition in a superconductor / quantum-dot / superconductor (S-QD-S) system by Green function method. We derive an equation to describe the Andreev bound states in S-QD-S system, and provide a unified understanding of the π -junction transition caused by three different mechanisms: (1) *Zeeman splitting*. For QD with two spin levels E_{\uparrow} and E_{\downarrow} , we find that the surface of the Josephson current $I(\phi = \frac{\pi}{2})$ vs the configuration of $(E_{\uparrow}, E_{\downarrow})$ exhibits interesting profile: a sharp peak around $E_{\uparrow} = E_{\downarrow} = 0$; a positive ridge in the region of $E_{\uparrow} \cdot E_{\downarrow} > 0$; and a *negative*, flat, shallow plain in the region of $E_{\uparrow} \cdot E_{\downarrow} < 0$. (2) *Intra-dot interaction*. We deal with the intra-dot Coulomb interaction by Hartree-Fock approximation, and find that the system behaves as a π -junction when QD becomes a magnetic dot due to the interaction. The conditions for π -junction transition are also discussed. (3) *Non-equilibrium distribution*. We replace the Fermi distribution $f(\omega)$ by a non-equilibrium one $\frac{1}{2} [f(\omega - V_c) + f(\omega + V_c)]$, and allow Zeeman splitting in QD where $E_{\uparrow} = -E_{\downarrow} = h$. The curves of $I(\phi = \frac{\pi}{2})$ vs V_c show the novel effect of interplay of non-equilibrium distribution with magnetization in QD.

I. INTRODUCTION

Superconductivity has the nature of quantum condensation in a macroscopic scale, which can be described by a wavefunction with phase factor $e^{i\phi}$. When two superconductors are weak linked, the phase difference will manifest in the dc Josephson current, with the current-phase relation $I = I_c \sin(\phi_1 - \phi_2)$. If the weak link area is controlled by certain external conditions, the magnitude of the critical current I_c may be either suppressed [1] or enhanced [2]. In some occasions, even the sign of I_c may be reversed [3], or equivalently the phase factor $\sin(\phi_1 - \phi_2)$ changes to $\sin(\phi_1 - \phi_2 + \pi)$, referred to as the π -junction transition. One of the simplest example is the so-called superconducting quantum diffraction, in which a superconductor / insulator / superconductor tunnel junction is tuned by an external magnetic field. The dc Josephson current vs the magnetic flux Φ_B has the form $I = I_c \left[\frac{\sin \pi \Phi_B / \Phi_0}{\pi \Phi_B / \Phi_0} \right] \sin(\phi_1 - \phi_2)$, and changes its sign at every Φ_B / Φ_0 equal to an integer. Unfortunately, the π -junction transition cannot be directly detected in the two terminal tunnel junction because the current source is used in the measurement to control supercurrent rather than phase difference. However, in a mesoscopic superconductor / normal-metal / superconductor (SNS) junction with the N-region coupled to normal electrode(s) [4,5], the phase difference can be determined independently by the coherent Andreev reflection current which is proportional to $|e^{i\phi_1} + e^{i\phi_2}|^2 = 2[1 + \cos(\phi_1 - \phi_2)]$. Thus, direct observation of the π -junction transition becomes accessible.

In mesoscopic SNS junctions, supercurrent is conducted through the N-region by Andreev reflection (AR) process [6]. The energy gaps of two superconducting electrodes serve as two "mirrors", reflecting electron into hole and hole into electron. For ballistic SNS junctions, discrete Andreev bound states are formed in the N-region, each state carries positive or negative supercurrent. For diffusive SNS junctions, the so-called current carrying density of states (CCDOS) plays the similar role, which also has positive and negative contributions to the supercurrent. Recent experiment [3] demonstrated the π -junction transition in the diffusive SNS junction by applying control voltage on the N-region. In fact, the biased normal reservoirs across mesoscopic N-region induce a non-equilibrium distribution in the N-region, and make the occupied fraction of CCDOS deviating from the equilibrium one. When the control voltage is excess a certain value, the non-equilibrium distribution has so

much weight on the negative part of CCDOS that the total current reverses its sign. Many theoretical works have been addressed on this issue, either for ballistic SNS junctions [7–9], or for diffusive SNS junctions [11–14].

In addition to non-equilibrium distribution, there is a completely different mechanism to realize the π -junction transition, i.e., coupling superconductors by an Anderson impurity or an interacting quantum dot (QD). The works of Glazman *et al.* [15] and Spivak *et al.* [16] revealed that when the impurity is single occupied, the sign of Josephson current for infinite Coulomb repulsion is opposite to that without the repulsion. Ishizaka *et al.* [17] obtained the condition for π -junction transition, by using non-crossing approximation and varying the strength of the Coulomb repulsion, the bare level position, the tunneling strength, and the temperature. Rozhkov *et al.* [18] analyzed the system in a non-perturbative way, and found a novel intermediate phase in which one of $\phi = 0$ and $\phi = \pi$ is stable while the other is metastable, with the energy $E(\phi)$ having a kink somewhere in between. Clerk *et al.* [19] studied the case of infinite- U and the regime where the superconducting gap Δ and the Kondo temperature T_K are comparable, showing that the position of the sub-gap resonance in the impurity spectral function develops a strong anomalous phase dependence, and the π -junction behavior is lost as the position of the bound state moves above the Fermi energy.

Recently, there are growing interests in the physics of superconductor in contact with ferromagnetic material, and the following works revealed another approach to achieve π -junction. Prokić *et al.* [20] presented a theory of the π -junction transition in atomic-scale superconductor / ferromagnet (S/F) superlattices. They found that the critical Josephson current has a non-monotonic dependence on the exchange field h in the ferromagnetic layer, becoming zero at the critical value, corresponding to the transition between $\phi = 0$ and $\phi = \pi$ in the ground state. Yip *et al.* [21] and Heikkilä *et al.* [22] demonstrated that the supercurrent through a mesoscopic SFS junction oscillates with an exponential decreasing envelope as a function of the exchange field or the distance between the electrodes. They also proposed that the suppressed supercurrent by the exchange field can be recovered by a proper non-equilibrium distribution.

With these in mind, we are curious whether there is any relationship among the above three mechanisms for π -junction transition. Motivated by this question, we investigate the following cases of π -junction transition in a superconductor / quantum dot / superconductor (S-QD-S) system and provide a unified picture based on Andreev bound states. In section II, we study the π -junction transition caused by Zeeman splitting. Assuming the QD with

two spin levels E_\uparrow and E_\downarrow , we find that the surface of the Josephson current $I(\frac{\pi}{2})$ vs the configuration of $(E_\uparrow, E_\downarrow)$ exhibits interesting profile: a sharp peak around $E_\uparrow = E_\downarrow = 0$; a positive ridge in the region of $E_\uparrow \cdot E_\downarrow > 0$; and a *negative*, flat, shallow plain in the region of $E_\uparrow \cdot E_\downarrow < 0$. In section III, we study the π -junction transition caused by intra-dot interaction. We model QD by $H_{dot} = E_0 \sum_\sigma c_\sigma^\dagger c_\sigma + U n_\uparrow n_\downarrow$, and handle the interaction term by Hartree-Fock approximation. Thus this case is reduced to the first one except a self-consistent calculation for $\langle n_\sigma \rangle$. We show that the π -junction transition occurs when QD becomes a magnetic dot due to the interaction. The conditions for π -junction transition are also discussed. In section IV, we study the π -junction transition caused by non-equilibrium distribution in QD. By replacing the Fermi distribution $f(\omega)$ with a non-equilibrium one $\frac{1}{2} [f(\omega - V_c) + f(\omega + V_c)]$, and allowing Zeeman splitting in QD as $E_\uparrow = -E_\downarrow = h$, we find that for $h = 0$, the supercurrent reverses its sign when control voltage V_c is excess a certain value, which is agree with previous work [24] and the experiment [3]. For $h \neq 0$, the curves of Josephson current vs control voltage show a novel effect of interplay of non-equilibrium distribution with the magnetization in QD. Finally, we summarize our understanding of π -junction transition in S-QD-S system in section V.

II. QD WITH TWO SPIN LEVELS

A. model Hamiltonian and formulation

In this section, we study the S-QD-S system modeled by the following Hamiltonian:

$$\begin{aligned}
H &= H_L + H_R + H_{dot} + H_T \quad , \\
H_L &= \sum_{k\sigma} \epsilon_k a_{k\sigma}^\dagger a_{k\sigma} + \sum_k \left[\Delta e^{-i\phi_L} a_{k\uparrow}^\dagger a_{-k\downarrow}^\dagger + h.c \right] \quad , \\
H_R &= \sum_{p\sigma} \epsilon_p b_{p\sigma}^\dagger b_{p\sigma} + \sum_p \left[\Delta e^{-i\phi_R} b_{p\uparrow}^\dagger b_{-p\downarrow}^\dagger + h.c \right] \quad , \\
H_{dot} &= \sum_\sigma E_\sigma c_\sigma^\dagger c_\sigma \quad , \\
H_T &= \sum_{k\sigma} \left[t_L a_{k\sigma}^\dagger c_\sigma + h.c \right] + \sum_{p\sigma} \left[t_R b_{p\sigma}^\dagger c_\sigma + h.c \right] \quad ,
\end{aligned} \tag{1}$$

where H_L, H_R describe the left and right superconducting leads with phase difference $\phi_L - \phi_R$ [29], H_{dot} describes the quantum dot with two spin levels, and H_T is the coupling between the quantum dot and the superconducting leads.

Since Josephson current can be expressed in terms of the Green functions of the QD, we first derive the Green function by solving Dyson equation. Following the formulation in [23], we denote \mathbf{G} and \mathbf{g} as the Green functions of QD in Nambu representation, with and without the coupling to leads, respectively; and denote Σ as the self-energy due to the coupling between QD and the leads. The retarded Green function (Fourier transformed) of isolated QD is

$$\mathbf{g}^r = \begin{pmatrix} \frac{1}{\omega - E_{\uparrow} + i0^+} & 0 \\ 0 & \frac{1}{\omega + E_{\downarrow} + i0^+} \end{pmatrix}. \quad (2)$$

The retarded self-energy (Fourier transformed) under the wide bandwidth approximation can be derived as [23],

$$\Sigma_{L/R}^r(\omega) = -\frac{i}{2}\Gamma_{L/R}\rho(\omega) \begin{pmatrix} 1 & -\frac{\Delta}{\omega}e^{-i\phi_{L/R}} \\ -\frac{\Delta}{\omega}e^{i\phi_{L/R}} & 1 \end{pmatrix}. \quad (3)$$

where $\Gamma_{L/R}$ is the coupling strength between the superconducting leads and QD, defined by $\Gamma_{L/R} \equiv 2\pi N_{L/R} t_{L/R}^2$, in which N_L and N_R are the density of states in the left and right leads in normal state. The factor $\rho(\omega)$ is defined as,

$$\rho(\omega) \equiv \begin{cases} \frac{|\omega|}{\sqrt{\omega^2 - \Delta^2}} & |\omega| > \Delta \\ \frac{\omega}{i\sqrt{\Delta^2 - \omega^2}} & |\omega| < \Delta \end{cases}. \quad (4)$$

Notice that $\rho(\omega)$ is the ordinary dimensionless BCS density of states when $|\omega| > \Delta$, but has an imaginary part when $|\omega| < \Delta$, corresponding to Andreev reflection process within the superconducting gap. For simplicity, we assume that the two superconducting leads are identical except a phase difference. Let $\phi_L = \frac{\phi}{2}$, $\phi_R = -\frac{\phi}{2}$, $\Gamma_L = \Gamma_R \equiv \Gamma$, then we obtain

$$\Sigma^r \equiv \Sigma_L^r + \Sigma_R^r = -i\Gamma\rho(\omega) \begin{pmatrix} 1 & -\frac{\Delta}{\omega}\cos\frac{\phi}{2} \\ -\frac{\Delta}{\omega}\cos\frac{\phi}{2} & 1 \end{pmatrix}, \quad (5)$$

$$\tilde{\Sigma}^r \equiv \Sigma_L^r - \Sigma_R^r = -i\Gamma\rho(\omega) \begin{pmatrix} 0 & -\frac{\Delta}{\omega}(-i)\sin\frac{\phi}{2} \\ -\frac{\Delta}{\omega}i\sin\frac{\phi}{2} & 0 \end{pmatrix}. \quad (6)$$

By using Dyson equation, the retarded Green function of QD can be obtained as,

$$\mathbf{G}^r = [\mathbf{g}^{r^{-1}} - \Sigma^r]^{-1} = \frac{1}{A} \begin{pmatrix} g_{22}^{r^{-1}} - \Sigma_{22}^r & \Sigma_{12}^r \\ \Sigma_{21}^r & g_{11}^{r^{-1}} - \Sigma_{11}^r \end{pmatrix}, \quad (7)$$

where $A = A(\omega)$ defined as

$$A(\omega) \equiv \det \left[\mathbf{g}^{r^{-1}} - \mathbf{\Sigma}^r \right] = (g_{22}^{r^{-1}} - \Sigma_{22}^r)(g_{11}^{r^{-1}} - \Sigma_{11}^r) - \Sigma_{12}^r \Sigma_{21}^r . \quad (8)$$

The general current formula for a mesoscopic hybrid multi-terminal system has been derived in [23]. For the time-independent case and QD with two spin levels under consideration, the current formula can be rewritten in a compact form (in units of $e = \hbar = 1$):

$$I_{L/R} = I_{L/R,\uparrow} + I_{L/R,\downarrow} = \int \frac{d\omega}{2\pi} 2 \operatorname{Re} \left[\mathbf{G} \mathbf{\Sigma}_{L/R} \right]_{11-22}^< , \quad (9)$$

where $[CD]^< \equiv C^< D^a + C^r D^<$, $[]_{11-22} \equiv []_{11} - []_{22}$, and \mathbf{G} , $\mathbf{\Sigma}_{L/R}$ are the Fourier transformed 2×2 Nambu matrices. Since $I = I_L = -I_R$ in the stationary transport, the current formula can be further reduced to

$$I = \frac{1}{2}(I_L - I_R) = \int \frac{d\omega}{2\pi} \operatorname{Re} \left[\mathbf{G} \tilde{\mathbf{\Sigma}} \right]_{11-22}^< , \quad (10)$$

with $\tilde{\mathbf{\Sigma}} \equiv \mathbf{\Sigma}_L - \mathbf{\Sigma}_R$. Applying the fluctuation-dissipation theorem, one has $\mathbf{G}^< = f(\omega) [\mathbf{G}^a - \mathbf{G}^r]$ and $\tilde{\mathbf{\Sigma}}^< = f(\omega) [\tilde{\mathbf{\Sigma}}^a - \tilde{\mathbf{\Sigma}}^r]$, where $f(\omega) = 1/(e^{\beta\omega} + 1)$ is the Fermi distribution function. Notice that $(\mathbf{G}^r)^\dagger = \mathbf{G}^a$, $(\tilde{\mathbf{\Sigma}}^r)^\dagger = \tilde{\mathbf{\Sigma}}^a$, the expression in the integrand can be simplified to

$$\operatorname{Re} \left[\mathbf{G} \tilde{\mathbf{\Sigma}} \right]_{11-22}^< = f(\omega) 2 \sin \phi \frac{\Gamma^2 \Delta^2}{\omega^2 - \Delta^2} \left[-\operatorname{Im} \frac{1}{A(\omega)} \right] . \quad (11)$$

Consequently, the Josephson current is expressed as

$$I = 2 \sin \phi \int \frac{d\omega}{2\pi} f(\omega) j(\omega) , \quad (12)$$

in which the current carrying density of states (CCDOS) $j(\omega)$ is defined by

$$j(\omega) \equiv \frac{\Gamma^2 \Delta^2}{\omega^2 - \Delta^2} \left[-\operatorname{Im} \frac{1}{A(\omega)} \right] . \quad (13)$$

Because the singularities of $j(\omega)$ lie in the same half-plane, CCDOS $j(\omega)$ satisfies the condition $\int j(\omega) d\omega = 0$.

Since $\Sigma^r(\omega)$ is purely imaginary when $|\omega| > \Delta$ while purely real when $|\omega| < \Delta$, so $A(\omega)$ has finite imaginary part when $|\omega| > \Delta$, while infinitesimal imaginary part when $|\omega| < \Delta$. Correspondingly, the Josephson current can be divided into two parts, contributed from the continuous spectrum and from the discrete spectrum, respectively:

$$\begin{aligned}
I &= I_c + I_d , \\
I_c &\equiv 2 \sin \phi \left(\int_{-\infty}^{-\Delta} + \int_{\Delta}^{\infty} \right) \frac{d\omega}{2\pi} f(\omega) j(\omega) , \\
I_d &\equiv 2 \sin \phi \int_{-\Delta}^{\Delta} \frac{d\omega}{2\pi} f(\omega) j(\omega) .
\end{aligned} \tag{14}$$

We shall show in the appendix that when $|\omega| < \Delta$ and $\phi \neq 0$, the equation $A(\omega) = 0$ has two real roots denoted by $\tilde{E}_1 = \Delta \sin \theta_1$ and $\tilde{E}_2 = \Delta \sin \theta_2$, where θ_1 and θ_2 are the two roots of the following equation,

$$\left(\sin \theta + \frac{\Gamma}{\Delta} \tan \theta - \frac{E_{\uparrow}}{\Delta} \right) \left(\sin \theta + \frac{\Gamma}{\Delta} \tan \theta + \frac{E_{\downarrow}}{\Delta} \right) \cos^2 \theta - \frac{\Gamma^2}{\Delta^2} \cos^2 \frac{\phi}{2} = 0 \tag{15}$$

with $\theta \in (-\frac{\pi}{2}, \frac{\pi}{2})$. Equation (15) completely determines the properties of Andreev bound states. The roots \tilde{E}_1 and \tilde{E}_2 are just the Andreev bound states. In the range of $|\omega| < \Delta$, $A(\omega)$ can be written as $a(\omega)(\omega - \tilde{E}_1 + i0^+)(\omega - \tilde{E}_2 + i0^+)$, and $\left[-\text{Im} \frac{1}{A(\omega)} \right]$ is reduced to

$$-\text{Im} \frac{1}{A(\omega)} = \pi \left[\frac{1}{A'(\tilde{E}_1)} \delta(\omega - \tilde{E}_1) + \frac{1}{A'(\tilde{E}_2)} \delta(\omega - \tilde{E}_2) \right] . \tag{16}$$

Finally, the Josephson current through S-QD-S system can be expressed as,

$$\begin{aligned}
I &= I_c + I_d , \\
I_c &\equiv 2 \sin \phi \left(\int_{-\infty}^{-\Delta} + \int_{\Delta}^{\infty} \right) \frac{d\omega}{2\pi} f(\omega) \frac{\Gamma^2 \Delta^2}{\omega^2 - \Delta^2} \left[-\text{Im} \frac{1}{A(\omega)} \right] , \\
I_d &\equiv \sin \phi \left[f(\tilde{E}_1) \frac{\Gamma^2 \Delta^2}{\tilde{E}_1^2 - \Delta^2} \frac{1}{A'(\tilde{E}_1)} + f(\tilde{E}_2) \frac{\Gamma^2 \Delta^2}{\tilde{E}_2^2 - \Delta^2} \frac{1}{A'(\tilde{E}_2)} \right] .
\end{aligned} \tag{17}$$

This current formula will be used in the following numerical study [30].

B. numerical results and discussions

Now we discuss the numerical results for Andreev bound states and the Josephson current. In all numerical studies of this paper, we take $e = \hbar = k_B = 1$, set $\Delta = 1$, i.e., measure all energies in units of Δ , let $\Gamma = 0.1$ for symmetric and weak coupling case, and fix the phase difference $\phi = \frac{\pi}{2}$.

Fig.1 presents the solution of Eq.(15), i.e., Andreev bound states of S-QD-S system. In the limit of $\Gamma \rightarrow \infty$, Eq.(15) gives $\tilde{E}_1 = |\cos \frac{\phi}{2}|$ and $\tilde{E}_2 = -|\cos \frac{\phi}{2}|$, the well-known Andreev bound states for a clean superconducting point contact [10]. Conversely, in the limit of $\Gamma \rightarrow 0$, the two roots of Eq.(15) are $\tilde{E}_1 = E_{\uparrow}$ and $\tilde{E}_2 = -E_{\downarrow}$, i.e., the bare levels

of electron with spin \uparrow and hole with spin \downarrow of the QD. (We describe spin \uparrow quasiparticle in electron language and spin \downarrow quasiparticle in hole language due to the choice of Nambu representation.) For the case of $\Gamma \ll \Delta$ under consideration, where QD is weakly coupled with the superconducting leads, the solutions of Eq.(15) depend strongly on the configuration of QD levels $(E_\uparrow, E_\downarrow)$, but weakly on the phase difference ϕ . The surfaces of \tilde{E}_1 vs $(E_\uparrow, E_\downarrow)$ and \tilde{E}_2 vs $(E_\uparrow, E_\downarrow)$ for $\phi = \frac{\pi}{2}$ are shown in Fig.1a and Fig.1b, respectively. In this case, the electron level E_\uparrow and the hole level $-E_\downarrow$ are coupled by AR tunneling. Therefore, Andreev bound states can be viewed as hybrid states of E_\uparrow and $-E_\downarrow$, and an energy gap of the order Γ is opened where E_\uparrow and $-E_\downarrow$ are equal (see Fig.1c and Fig.1d). Further study on the relations of \tilde{E}_1 vs ϕ and \tilde{E}_2 vs ϕ can provide the information of supercurrent carried by each Andreev bound state (not shown).

Fig.2 presents the surface of Josephson current I vs the configuration of $(E_\uparrow, E_\downarrow)$. First, the surface is symmetric to the diagonal lines of $E_\uparrow = E_\downarrow$ and $E_\uparrow = -E_\downarrow$, which reflects the symmetry between electron and hole and the fact that supercurrent are non-spin-polarized. Second, the surface exhibits interesting profile: a sharp peak around $E_\uparrow = E_\downarrow = 0$; a positive ridge in the region of $E_\uparrow \cdot E_\downarrow > 0$; and a negative, flat, shallow plain in the region of $E_\uparrow \cdot E_\downarrow < 0$. Note that the positive ridge and negative plain share a sharp edge. Third, consider two special but typical cases, $E_\uparrow = E_\downarrow \equiv E_0$ (Fig.2b), and $E_\uparrow = -E_\downarrow \equiv E_0$ (Fig.2c), which are actually the diagonal cuts of Fig.2a. For the case of $E_\uparrow = E_\downarrow$, the I vs E_0 curve has a peak at $E_0 = 0$ with a width of Γ , which reproduces the result for QD with one spin-degenerate level [24]. For the case of $E_\uparrow = -E_\downarrow$, the I vs E_0 curve has the same maximum at $E_0 = 0$, but jumps suddenly from the positive maximum to a small negative value around $E_0 = \pm\Gamma$, which is quite similar to the curve of the critical current vs the exchange field in an atomic scale S/F superlattice (see Fig.2 of [20]).

To understand these features, we plot CCDOS $j(\omega)$ for different configurations of $(E_\uparrow, E_\downarrow)$ in Fig.3. The supercurrent can be expressed as $I = 2 \sin \phi \int \frac{d\omega}{2\pi} f(\omega) j(\omega)$, and only the spectrum of $\omega < 0$ devotes to the current at zero temperature. For the spectrum of $E_\uparrow = E_\downarrow = 0$, $j(\omega)$ has two δ -function type discrete spectrum within the superconducting gap, corresponding to two Andreev bound states. They carry supercurrent with opposite signs, positive for $\tilde{E}_1 < 0$, and negative for $\tilde{E}_2 > 0$. $j(\omega)$ also has continuous spectrum outside the superconducting gap, negative and positive for $\omega < -\Delta$ and $\omega > \Delta$, respectively. Since the contribution from the discrete spectrum is much larger than that from the continuous one, the current peak at $E_\uparrow = E_\downarrow = 0$ is mostly contributed from \tilde{E}_1 . For the spectrum

of $E_{\uparrow} = E_{\downarrow} = E_0 \neq 0$, \tilde{E}_1 and \tilde{E}_2 move toward $\pm\Delta$, symmetric to the Fermi surface (see also Fig.1c). The contribution from the discrete spectrum \tilde{E}_1 decreases continuously with E_0 , corresponding to the Γ -width broadening of the $E_0 = 0$ peak in Fig.2c. For the spectrum of $E_{\uparrow} = -E_{\downarrow} = E_0 \neq 0$, however, \tilde{E}_1 and \tilde{E}_2 move in the same direction. When $E_0 < -\Gamma$ or $E_0 > \Gamma$, both \tilde{E}_1 and \tilde{E}_2 are below or above the Fermi surface (see also Fig.1d). As a consequence, they have little net contribution to the supercurrent, and the relatively small negative continuous spectrum of $\omega < -\Delta$ dominates. Because the crossover of \tilde{E}_1 and \tilde{E}_2 from different sides of the Fermi surface to one side occurs abruptly, sudden jumps between the positive maximum and the negative valleys appear in Fig.2d. Similarly, one can understand the whole surface of Fig.2 with the help of the Andreev bound states in Fig.1 and the properties of CCDOS in Fig.3.

The above results are for zero temperature, the temperature dependence of the Josephson current is shown in Fig.4. Notice that the supercurrent is sensitive to the temperature. The height of $E_{\uparrow} = E_{\downarrow} = 0$ peak (referred as I_0) decreases rapidly with the increase of the temperature, $I_0 = 0.06, 0.004, 0.001$ for $T = 0, 0.25, 0.50$, respectively. The sharp edge between $I > 0$ and $I < 0$ is also smeared out at finite temperatures. This reason is, at finite temperature not only the Andreev bound state below the Fermi surface but also the one above the Fermi surface has contribution to the supercurrent.

III. QD WITH INTRA-DOT INTERACTION

A. Hartree-Fock approximation

In this section, we investigate the π -junction transition caused by the intra-dot interaction. The quantum dot with Coulomb interaction can be described by $H_{dot} = E_0 \sum_{\sigma} c_{\sigma}^{\dagger} c_{\sigma} + U n_{\uparrow} n_{\downarrow}$. As in the problem of local moment in nonmagnetic metals [26], we deal with the interaction term by Hartree-Fock approximation (HFA), in which $U n_{\uparrow} n_{\downarrow}$ is replaced by $U \langle n_{\uparrow} \rangle n_{\downarrow} + U n_{\uparrow} \langle n_{\downarrow} \rangle$. Thus, H_{dot} becomes $\sum_{\sigma} E'_{\sigma} c_{\sigma}^{\dagger} c_{\sigma}$, with the effective levels $E'_{\sigma} \equiv E_0 + U \langle n_{\bar{\sigma}} \rangle$. Despite of the roughness of HFA, it contains the physics of magnetization due to Coulomb interaction. More important, the approximation allows us to obtain a solution including infinite order of tunneling processes, which is crucial for describing the Andreev bound states and the supercurrent they carried. However, HFA fails in the Kondo regime. As discussed in [19], if $\Delta \ll T_K \equiv \sqrt{UT} e^{-\pi|E_0 - \mu|/\Gamma}$, the spin of the impurity is com-

pletely screened by Kondo effect, and there will be no π -junction behavior. In this work, we will constrain ourselves to the weak coupling case where magnetization effect dominates, corresponding to $\Delta \gg T_K$ regime.

Then most of the formula in the previous section can be transplanted, except the averaged occupation number $\langle n_\sigma \rangle$ needs a self-consistent calculation. Notice that $\langle n_\sigma \rangle$ can be derived from the retarded Green function of QD as

$$\langle n_\uparrow \rangle = \int \frac{d\omega}{2\pi} f(\omega) [-2 \text{Im} G_{11}^r(\omega)] , \quad (18)$$

$$1 - \langle n_\downarrow \rangle = \int \frac{d\omega}{2\pi} f(\omega) [-2 \text{Im} G_{22}^r(\omega)] . \quad (19)$$

Similar to the current formula, $\langle n_\sigma \rangle$ can be divided into two parts, the contribution from discrete spectrum and the contribution from continuous spectrum,

$$\begin{aligned} \langle n_\uparrow \rangle &= \langle n_\uparrow \rangle_c + \langle n_\uparrow \rangle_d , \\ \langle n_\uparrow \rangle_c &= \left(\int_{-\infty}^{-\Delta} + \int_{\Delta}^{\infty} \right) \frac{d\omega}{2\pi} f(\omega) \left[-2 \text{Im} \frac{g_{22}^{r-1}(\omega) - \Sigma_{22}^r(\omega)}{A(\omega)} \right] , \\ \langle n_\uparrow \rangle_d &= \sum_{i=1}^2 \left[f(\omega) \frac{1}{A'(\omega)} \left(g_{22}^{r-1}(\omega) - \Sigma_{22}^r(\omega) \right) \right]_{\omega=\tilde{E}_i} , \\ \langle n_\downarrow \rangle &= \langle n_\downarrow \rangle_c + \langle n_\downarrow \rangle_d , \\ 1 - \langle n_\downarrow \rangle_c &= \left(\int_{-\infty}^{-\Delta} + \int_{\Delta}^{\infty} \right) \frac{d\omega}{2\pi} f(\omega) \left[-2 \text{Im} \frac{g_{11}^{r-1}(\omega) - \Sigma_{11}^r(\omega)}{A(\omega)} \right] , \\ 1 - \langle n_\downarrow \rangle_d &= \sum_{i=1}^2 \left[f(\omega) \frac{1}{A'(\omega)} \left(g_{11}^{r-1}(\omega) - \Sigma_{11}^r(\omega) \right) \right]_{\omega=\tilde{E}_i} . \end{aligned} \quad (20)$$

$$(21)$$

Since \mathbf{g}^r contains unknown quantity $\langle n_\sigma \rangle$ through E'_σ , the above equations for $\langle n_\sigma \rangle$ should be solved self-consistently.

B. numerical results and discussions

Next, we present the numerical results for the interacting QD system at zero temperature. Fig.5 shows I vs E_0 and corresponding $\langle n_\sigma \rangle$ vs E_0 curves for two typical cases, the QD without interaction ($U = 0$ in Fig.5a) and with strong interaction ($U \gg \Gamma$ in Fig.5b). The S-QD-S system behaves like one of the above two cases, Depending on the magnitudes of the interacting constant U and the coupling strength Γ , the S-QD-S system may behave differently. If $U < \Gamma$, the occupation numbers $\langle n_\uparrow \rangle$ and $\langle n_\downarrow \rangle$ are almost equal, leading to the

supercurrent always positive with a maximum at $E_0 = -U/2$, and the system behaves as same as the non-interacting one. On the contrast, if $U > \Gamma$, a symmetry breaking solution of Eq.(19) and Eq.(20) is energy preferred, in which $\langle n_\uparrow \rangle$ and $\langle n_\downarrow \rangle$ are unequal, and QD becomes a magnetic dot. Consequently, the effective level ($E'_\uparrow, E'_\downarrow$) occupy a series of configurations in the negative plain of Fig.1, so the Josephson current has a small but negative valley in I vs E_0 curve. We determine the transition border of the above two cases by the parametric diagram of I vs $(-E_0/\Gamma, \Gamma/U)$ in Fig.6. By virtue of electron-hole symmetry, the diagram is symmetric to $-E_0/U = 0.5$. The black area in Fig.6b indicates the range of parameters where the S-QD-S system behaves as a π -junction. One can see from the diagram that the system is likely to transfer to π -junction around $E_0 = -U/2$.

The temperature dependence are studied in Fig.7, which shows I vs E_0 curves with $U = 1$ for different temperatures. Due to the electron-hole symmetry, only half of the plot is shown. The sharp structure at zero temperature is smoothed at finite temperatures, and the negative part of the supercurrent vanishes above a critical temperature. These features can be understood by taking account of the temperature effect on the supercurrent through QD with two spin levels in Fig.4 and the temperature effect on the averaged QD occupation numbers. We also study the diagram of I vs (U, T) where E_0 is set to $-U/2$ (not shown here). The transition line from $I < 0$ to $I > 0$ can be fitted as $U = 0.17 + 7.5T$, which is consistent with the result derived by non-crossing approximation in [17].

IV. QD IN NON-EQUILIBRIUM DISTRIBUTION

Now we turn to discuss π -junction transition caused by non-equilibrium distribution in QD. In a recent work by Sun *et al.* [24], a mesoscopic four-terminal Josephson junction (S-QD-S with two normal leads connected to QD) was studied. By using non-equilibrium Green function method, they found that the supercurrent between the two superconducting electrodes can be suppressed and even reversed by changing the dc voltage applied across the two normal terminals. Here we only take the essential point of that work but omit its tedious calculation, by simply assuming that QD has a two-step distribution function as

$$F(\omega) = \frac{1}{2} [f(\omega - V_c) + f(\omega + V_c)] \xrightarrow{T \rightarrow 0} \begin{cases} 1 & \omega < -V_c \\ 0.5 & -V_c < \omega < V_c \\ 0 & \omega > V_c \end{cases}, \quad (22)$$

corresponding to the limit of $\Gamma_2 = \Gamma_4 \rightarrow 0$ in [24]. Different from [24], here we allow the two spin levels of QD have a Zeeman splitting, i.e., $E_\uparrow = -E_\downarrow = h$. The curves of the Josephson current $I(\phi = \frac{\pi}{2})$ vs the control voltage V_c for different Zeeman splitting h are shown in Fig.8. These curves are step-like because $F(\omega)$ is step-like at $T = 0$, and $j(\omega)$ has δ -function type discrete spectrum in the range of $-\Delta < \omega < \Delta$. Either finite temperature or small broadening of Andreev bound states will smooth the curves.

For $h = 0$, I reverses its sign around $V_c = \Gamma$, and the magnitude of positive current is much larger than that of negative one, which is agree qualitatively with the experiment [3] and previous work [24]. For $h \neq 0$, curves of I vs V_c have a peak around $V_c = h$, with the width about 2Γ , the height about half of that for $h = 0$. On each side of the peak, there is a negative current valley, where the system behaves as π -junction. These results are also consistent with the calculations for non-equilibrium SFS junction [21,22]. One can understand these curves by considering the two-step distribution $F(\omega)$ and CCDOS in Fig.4. For example, for the curve of $h = 0.2$ (marked with “1” in Fig.8), both positive and negative Andreev bound states are above the Fermi surface [see CCDOS of $(E_\uparrow, E_\downarrow) = (0.2, -0.2)$], located near $h - \Gamma$ and $h + \Gamma$, respectively. When $V_c = h$, the positive bound state has a weight of 0.5, while the negative one has 0, reducing the peak height to one half of that for $h = 0$. For both $V_c < h - \Gamma$ or $V_c > h + \Gamma$, the two Andreev bound states have the same weights (either 0 or 0.5), and have little net contribution to the supercurrent. Therefore, the negative continuous spectrum of $\omega < -\Delta$ is dominant in the supercurrent, leading to the π -junction transition on both sides of the positive peak.

V. CONCLUSIONS

In this work, we have investigated different mechanisms for the π -junction transition in S-QD-S system. From the current formula $I = 2 \sin \phi \int \frac{d\omega}{2\pi} F(\omega) j(\omega)$, one can see that the π -junction transition may originate from the change of CCDOS $j(\omega)$, or the change of the distribution function $F(\omega)$, or from the changes of both. The two mechanisms discussed in sections II and III, the Zeeman splitting and intra-dot interaction, are involved the change of CCDOS $j(\omega)$ only. These two mechanisms are closely connected since the intra-dot interaction may induce magnetization in QD if the interaction is strong enough. The third mechanism studied in section IV involves the change of the distribution function in QD, and the interplay of the magnetization with the non-equilibrium distribution in QD. It is

interesting that the change of CCDOS and the change of distribution have the similar effect on the π -junction transition, where the positive and negative Andreev bound states cancels each other, leaving the negative continuous spectrum dominant in the supercurrent. The interplay of the two mechanisms lead to the novel effect that the supercurrent suppressed by magnetization of the QD can be partially recovered by a proper non-equilibrium distribution of electrons in the QD.

ACKNOWLEDGMENTS

This project was supported by NSFC under grant No.10074001. One of the authors (T.-H. Lin) would also like to thank the support from the Visiting Scholar Foundation of State Key Laboratory for Mesoscopic Physics in Peking University.

* To whom correspondence should be addressed.

VI. APPENDIX

In this appendix, we discuss the equation of Andreev bound states, i.e. $A(\omega) = 0$ with $|\omega| < \Delta$:

$$A(\omega) = \left(\omega - E_{\uparrow} + \frac{\Gamma\omega}{\sqrt{\Delta^2 - \omega^2}} \right) \left(\omega + E_{\downarrow} + \frac{\Gamma\omega}{\sqrt{\Delta^2 - \omega^2}} \right) - \frac{\Gamma^2\Delta^2}{\Delta^2 - \omega^2} \cos^2 \frac{\phi}{2} = 0 \quad . \quad ((A1))$$

Let $\Gamma = \gamma\Delta$, $E_{\uparrow} = \varepsilon_1\Delta$, $E_{\downarrow} = -\varepsilon_2\Delta$, $\omega = \Delta \sin \theta$, $\theta \in (-\frac{\pi}{2}, \frac{\pi}{2})$, the equation becomes a dimensionless form,

$$b(\theta) \equiv (\sin \theta + \gamma \tan \theta - \varepsilon_1)(\sin \theta + \gamma \tan \theta - \varepsilon_2) \cos^2 \theta = \gamma^2 \cos^2 \frac{\phi}{2} \quad . \quad ((A2))$$

Note that the function of $y = \sin \theta + \gamma \tan \theta$ projects $\theta \in (-\frac{\pi}{2}, \frac{\pi}{2})$ monotonously to $y \in (-\infty, +\infty)$. One can find Θ_1 and Θ_2 in $(-\frac{\pi}{2}, \frac{\pi}{2})$, satisfying $\sin \Theta_1 + \gamma \tan \Theta_1 = \varepsilon_1$, and $\sin \Theta_2 + \gamma \tan \Theta_2 = \varepsilon_2$. Suppose $\Theta_1 < \Theta_2$, we have $b(\theta) \geq 0$ for $\theta \in (-\frac{\pi}{2}, \Theta_1] \cup [\Theta_2, \frac{\pi}{2})$, and $b(\theta) < 0$ for $\theta \in (\Theta_1, \Theta_2)$. Because $b(\pm\frac{\pi}{2}) = \gamma^2$, Eq.(A2) has at least two roots $\theta_1 \in (-\frac{\pi}{2}, \Theta_1]$ and $\theta_2 \in [\Theta_2, \frac{\pi}{2})$ for $\phi \neq 0$. It is straightforward to find the two roots by dichotomy method.

Next, we prove $b'(\theta) \geq 0$ for $0 < b(\theta) < \gamma^2$ and $\theta \in [\Theta_2, \frac{\pi}{2})$, while $b'(\theta) \leq 0$ for $0 < b(\theta) < \gamma^2$ and $\theta \in (-\frac{\pi}{2}, \Theta_1]$, so that θ_1 and θ_2 are the only two roots in $(-\frac{\pi}{2}, \Theta_1]$ and $[\Theta_2, \frac{\pi}{2})$. For $\theta \in [\Theta_2, \frac{\pi}{2})$, $\sin \theta + \gamma \tan \theta - \varepsilon_1 \geq 0$, and $\sin \theta + \gamma \tan \theta - \varepsilon_2 \geq 0$. Define

$x \equiv [(\sin \theta + \gamma \tan \theta - \varepsilon_1)(\sin \theta + \gamma \tan \theta - \varepsilon_2)]^{1/2}$, because $0 < b(\theta) < \gamma^2$, so one obviously has $0 < x < \gamma \sec \theta$.

$$\begin{aligned}
b'(\theta) &= 2(\sin \theta + \gamma \tan \theta - \frac{\varepsilon_1 + \varepsilon_2}{2})(\gamma + \cos^3 \theta) \\
&\quad - 2 \sin \theta \cos \theta (\sin \theta + \gamma \tan \theta - \varepsilon_1)(\sin \theta + \gamma \tan \theta - \varepsilon_2) \quad ((A3)) \\
&\geq 2x\gamma - 2 \cos \theta \cdot x^2 = -2 \cos \theta \cdot x(x - \gamma \sec \theta) \geq 0 \quad .
\end{aligned}$$

Therefore, Eq.(A2) has and only has two roots in the range of $\theta \in (-\frac{\pi}{2}, \frac{\pi}{2})$ for $\phi \neq 0$.

For $\phi = 0$, because $b'(\frac{\pi}{2}) = -2\gamma[2 - (\varepsilon_1 + \varepsilon_2)]$, $b'(-\frac{\pi}{2}) = 2\gamma[2 + (\varepsilon_1 + \varepsilon_2)]$, and considering the properties of $b'(\theta)$, one can clearly see that Eq.(A2) has two roots in $(-\frac{\pi}{2}, \frac{\pi}{2})$ if $|\varepsilon_1 + \varepsilon_2| < 2$, but only has one root in $(-\frac{\pi}{2}, \frac{\pi}{2})$ if $|\varepsilon_1 + \varepsilon_2| \geq 2$. However, this case is irrelevant to the Josephson effect.

REFERENCES

- [1] A. F. Morpurgo, T. M. Klapwijk, and B. J. van Wees, Appl. Phys. Lett. **72**, 966 (1999).
- [2] J. Kutchinsky, R. Taboryski, C. B. Sørensen, J. B. Hansen, and P. E. Lindelof, Phys. Rev. Lett. **83**, 4856 (1999).
- [3] J. J. Baselmans, A. F. Morpurgo, T. M. Klapwijk, and B. j. van Wees, Nature (London) **43**, 397 (1999).
- [4] H. Nakano and H. Takayanagi, Phys. Rev. B **47**, 7986 (1993).
- [5] H. T. Ilhan, H. V. Demir, and P. F. Bagwell, Phys. Rev. B **58**, 15120 (1998).
- [6] G. E. Blonder, M. Tinkham, and T. M. Klapwijk, Phys. Rev. B **25**, 4515 (1982).
- [7] B. J. van Wees, K.-M. H. Lenssen, and C. J. P. M. Harmans, Phys. Rev. B **44**, 470 (1991).
- [8] G. Wendin and V. S. Shumeiko, Phys. Rev. B **53**, R6006 (1996).
- [9] L.-F. Chang and P. F. Bagwell, Phys. Rev. B **55**, 12678 (1997).
- [10] P. F. Bagwell, Phys. Rev. B **46**, 12573 (1992).
- [11] A. F. Volkov, Phys. Rev. Lett. **74**, 4730 (1995).
- [12] A. F. Volkov and H. Takayanagi, Phys. Rev. B **56**, 11184 (1997).
- [13] S.-K. Yip, Phys. Rev. B **58**, 5803 (1998).
- [14] F. K. Wilhelm, G. Schön, and A. D. Zaikin, Phys. Rev. Lett. **81**, 1682 (1998).
- [15] L. I. Glazman and K. A. Matveev, JETP Lett. **49**, 659 (1989).
- [16] B. I. Spivak and S. A. Kivelson, Phys. Rev. B **43**, 3740 (1991).
- [17] S. Ishizaka, J. sone, and T. Ando, Phys. Rev. B **52**, 8358 (1995).
- [18] A. V. Rozhkov and D. P. Arovas, Phys. Rev. Lett. **82**, 2788 (1999).
- [19] A. A. Clerk and V. Ambegaokar, cond-mat/9910201.
- [20] V. Prokić, A. I. Buzdin, and L. Dobrosavljević-Grujić, Phys. Rev. B **59**, 587 (1999).
- [21] S.-K. Yip, Phys. Rev. B **62**, R6127 (2000).

- [22] T. T. Heikkilä, F. K. Wilhelm, and G. Schön, cond-mat/0003383.
- [23] Q.-F. Sun, B.-G. Wang, and T.-H. Lin, Phys. Rev. B **61**, 4754 (2000).
- [24] Q.-F. Sun, J. wang, and T.-H. Lin, Phys. Rev. B **62**, 648 (2000).
- [25] J. C. Cuevas, Martín-Rodero, and A. L. Yeyati, Phys. Rev. Lett. **29**, 3486 (1997).
- [26] P. W. Anderson, Phys. Rev. **124**, 41 (1961).
- [27] A. D. Zaikin and G. F. Zharkov, Sov. Phys. JETP **51**, 364 (1980).
- [28] A. V. Tartakovskii and M. V. Fistul, Sov. Phys. JETP **67**, 1935(1988).
- [29] The phase factor is $e^{-i\phi}$ instead of $e^{i\phi}$ since we choose $e = 1$ instead of $e = -1$.
- [30] The contribution from the discrete spectrum can also be derived from the dipersion relation of Andreev bound states, $I_d = 2 \left[\frac{\partial \tilde{E}_1}{\partial \phi} f(\tilde{E}_1) + \frac{\partial \tilde{E}_2}{\partial \phi} f(\tilde{E}_2) \right]$.

FIGURE CAPTIONS

- Fig. 1** Solution of the equation for Andreev bound states. Parameters are: $\Delta = 1$, $\Gamma = 0.1$, $\phi = \frac{\pi}{2}$. (a) and (b) show the two roots \tilde{E}_1 and \tilde{E}_2 ($\tilde{E}_1 > \tilde{E}_2$) vs the configurations of QD levels $(E_\uparrow, E_\downarrow)$. (c) and (d) are the diagonal cuts of (a) and (b), showing \tilde{E}_1 and \tilde{E}_2 vs E_0 with $E_\uparrow = E_\downarrow \equiv E_0$ and $E_\uparrow = -E_\downarrow \equiv E_0$, respectively. \tilde{E}_1 and \tilde{E}_2 can be viewed as two hybrid levels of the electron level of $E = E_\uparrow$ and the hole level of $E = -E_\downarrow$. (\tilde{E}_1 , \tilde{E}_2 , E_\uparrow and E_\downarrow are marked as E1, E2, Eu and Ed in the plot, respectively.)
- Fig. 2** Surface of the Josephson current I vs the configuration of QD levels $(E_\uparrow, E_\downarrow)$. Parameters are: $\Delta = 1$, $\Gamma = 0.1$, $\phi = \frac{\pi}{2}$, $T = 0$. (a) is the surface graph, while (b), (c) are the diagonal cuts. (b) and (c) show I vs E_0 with $E_\uparrow = E_\downarrow \equiv E_0$ and $E_\uparrow = -E_\downarrow \equiv E_0$, respectively.
- Fig. 3** CCDOS $j(\omega)$ for different $(E_\uparrow, E_\downarrow)$ configurations. The row from up to down corresponds to $E_\uparrow = -0.2, 0, 0.2$, and the column from left to right corresponds to $E_\downarrow = -0.2, 0, 0.2$. Each of CCDOS contains two types of spectrum: the discrete spectrum in the range of $|\omega| < 1$ and the continuous spectrum in the range of $|\omega| > 1$. To illustrate discrete spectrum, we broaden δ functions by 0.01 in the plots.
- Fig. 4** Surfaces of Josephson current I vs $(E_\uparrow, E_\downarrow)$ configurations at different temperatures: $T = 10^{-4}, 0.25, 0.50$ for (a), (b) and (c), respectively. Other parameters are the same as Fig.1.
- Fig. 5** The Josephson current I and the averaged QD occupation number $\langle n_\sigma \rangle$ vs the bare QD level E_0 , for (a) QD without interaction and (b) QD with strong interaction. Parameters are: $\Delta = 1$, $\Gamma = 0.1$, $\phi = \frac{\pi}{2}$, $T = 0$, $U = 0$ for (a) and $U = 1$ for (b).
- Fig. 6** Parametric diagram of the Josephson current I vs parameters $x \equiv -E_0/U$ and $y \equiv \Gamma/U$. We set $\Delta = 1$, $\Gamma = 0.1$, $\phi = \frac{\pi}{2}$, $T = 0$, and change E_0 and U to obtain the surface graph in (a). The black area of (b) indicates the range of parameter where the S-QD-S system behaves as a π -junction.
- Fig. 7** Temperature dependence of the I vs E_0 . Parameters are: $\Delta = 1$, $\Gamma = 0.1$, $\phi = \frac{\pi}{2}$, $U = 1$; $T = 0.001, 0.05, 0.10, 0.15$, and 0.20 for curves marked by 1, 2, 3, 4, and 5, respectively.

Fig. 8 The Josephson current I vs the control voltage V_c for different Zeeman splitting of $E_{\uparrow} = -E_{\downarrow} = h$ in QD. Parameters are: $\Delta = 1$, $\Gamma = 0.1$, $\phi = \frac{\pi}{2}$, $T = 0$; $h = 0, 0.2, 0.4, 0.6$, and 0.8 for curves marked with 0, 1, 2, 3, and 4, respectively.

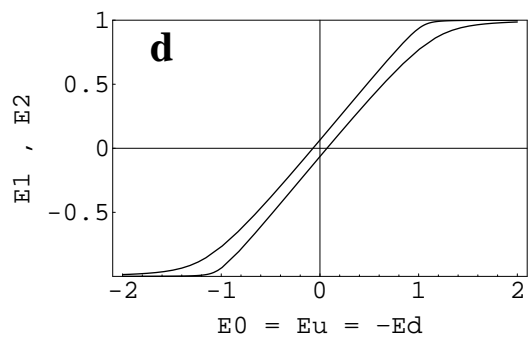
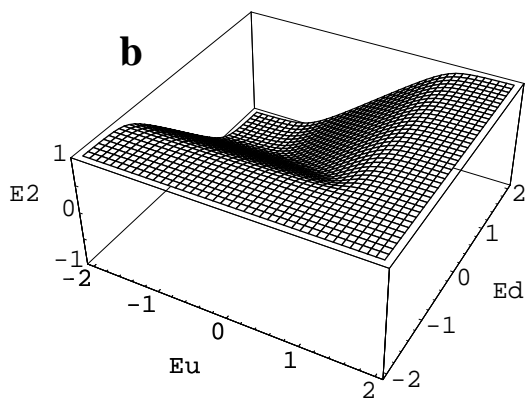
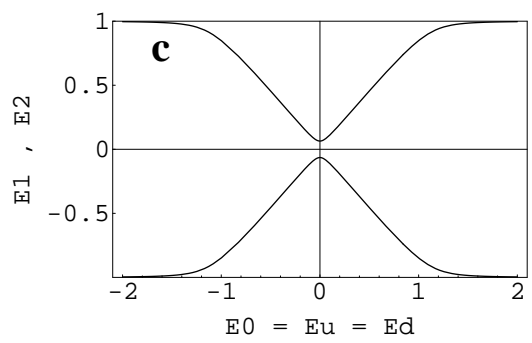
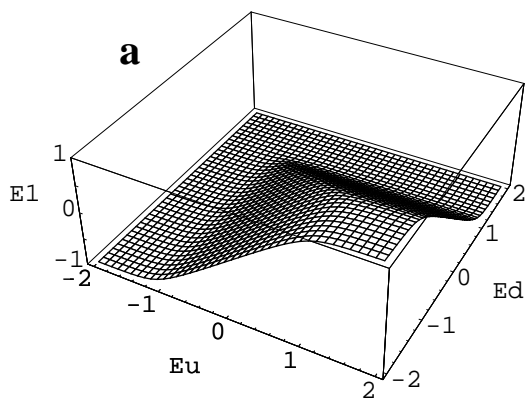


Fig.1

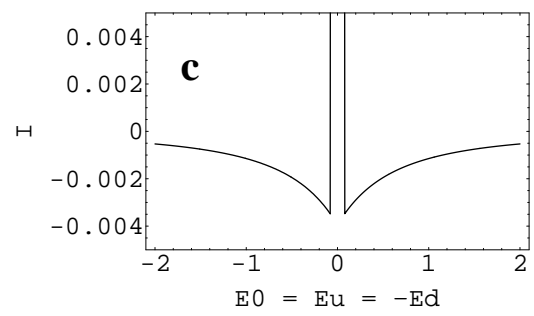
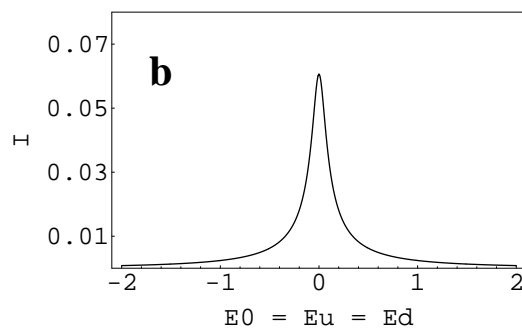
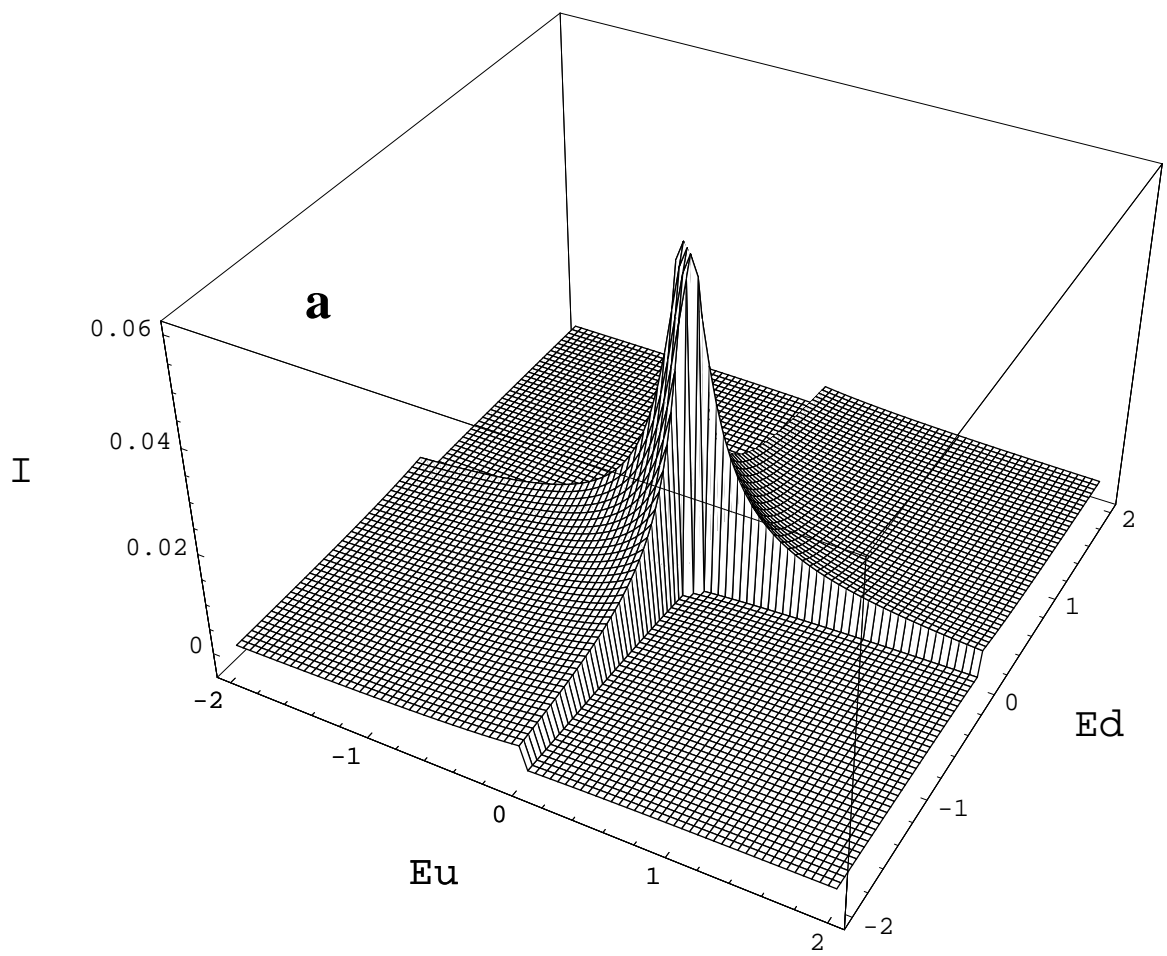


Fig.2

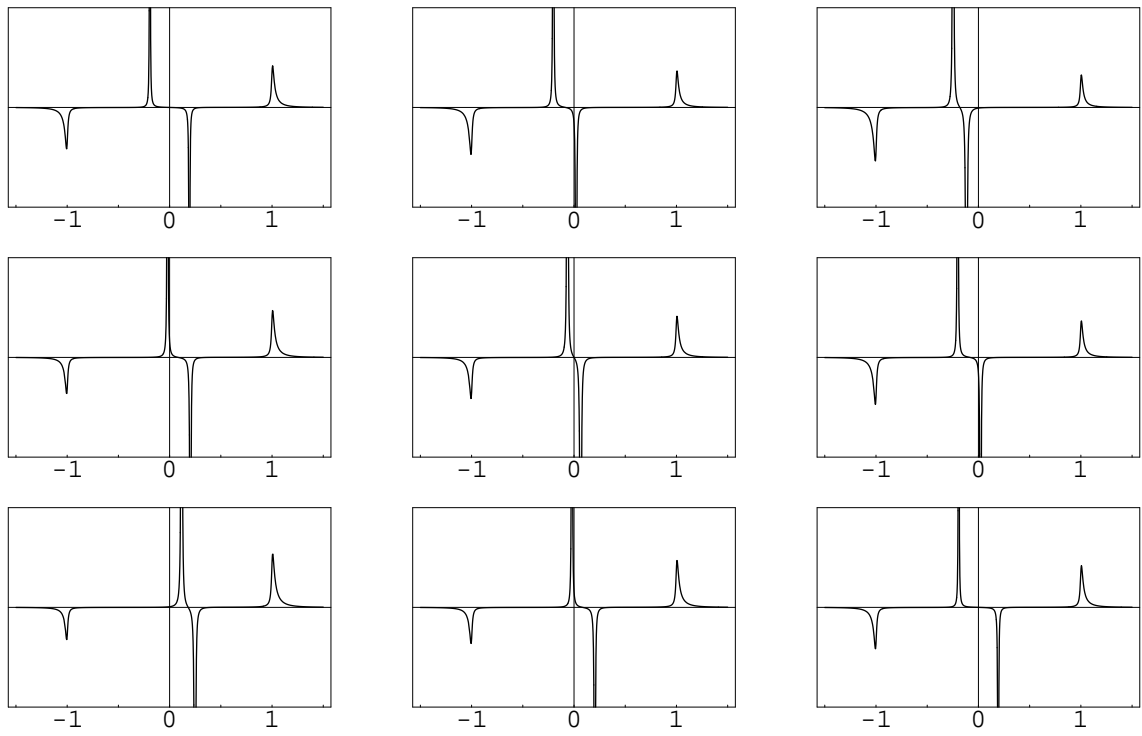


Fig.3

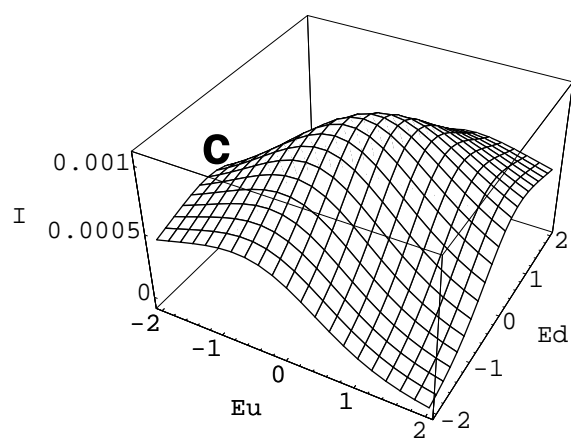
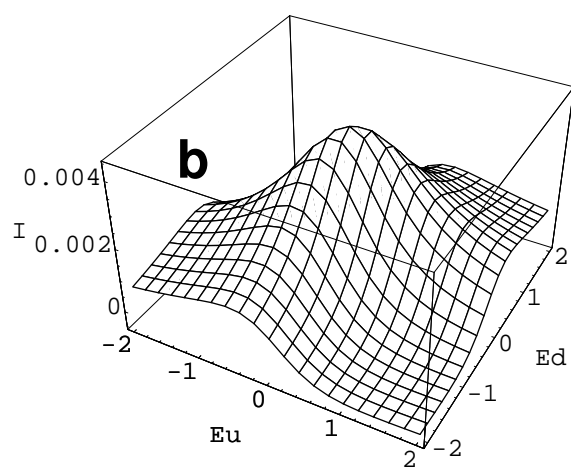
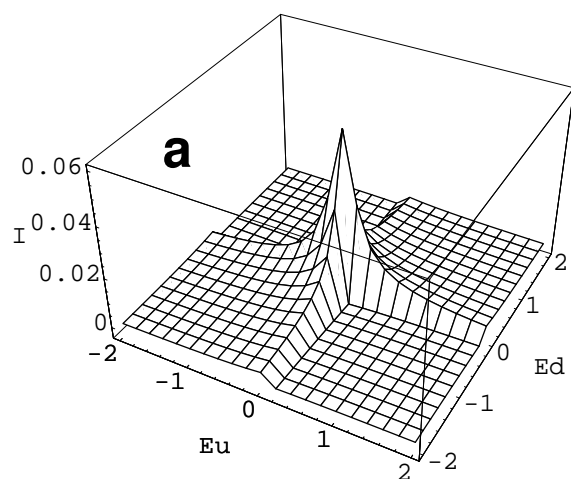


Fig.4

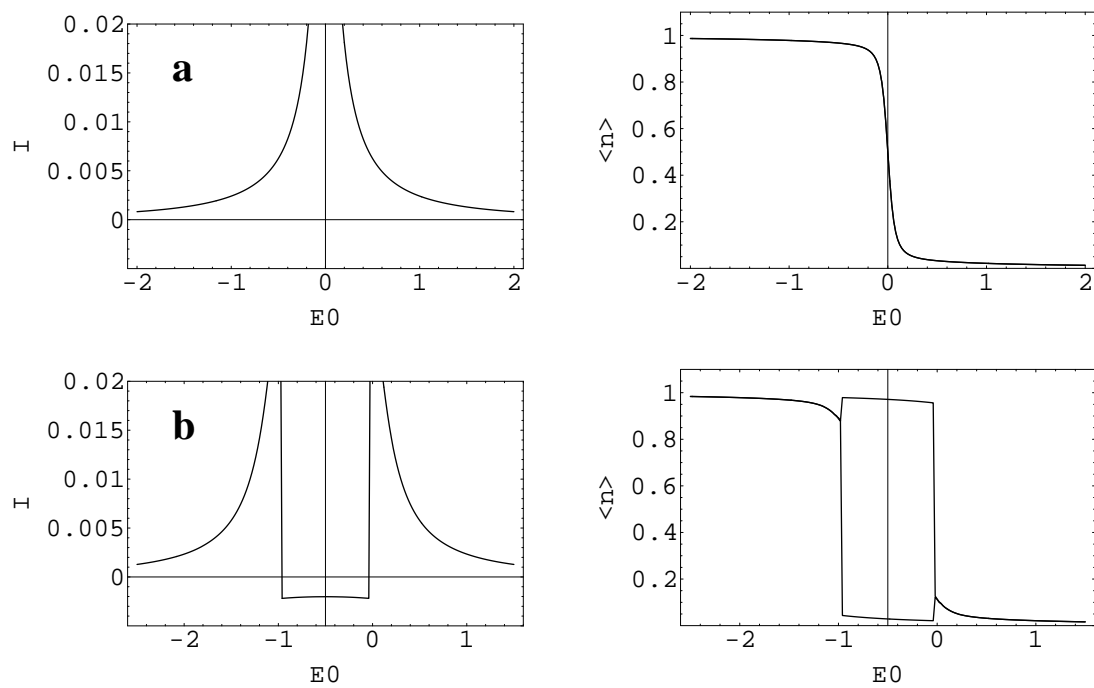


Fig.5

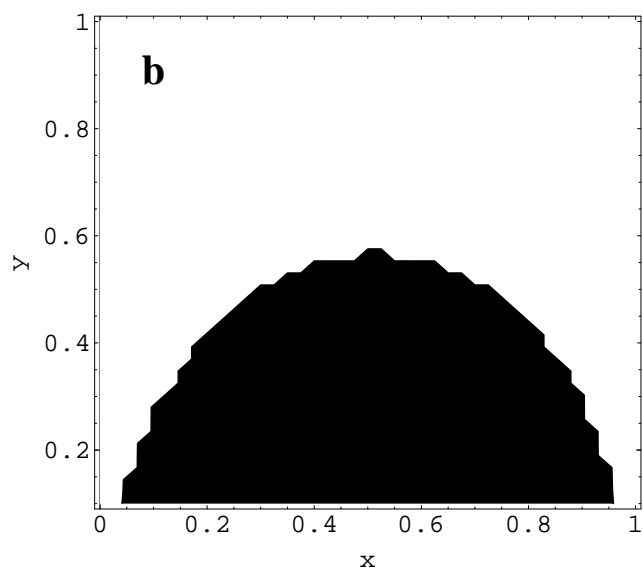
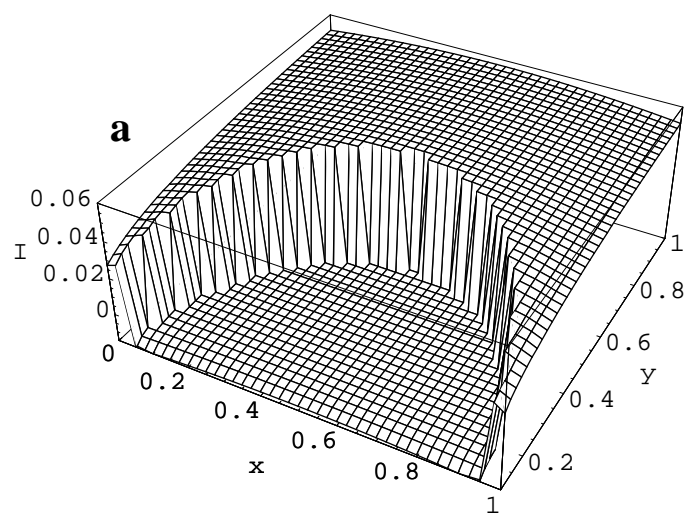


Fig.6

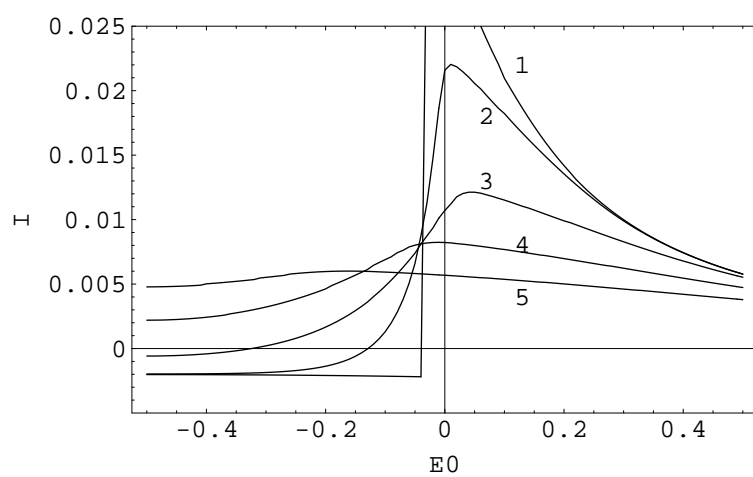


Fig.7

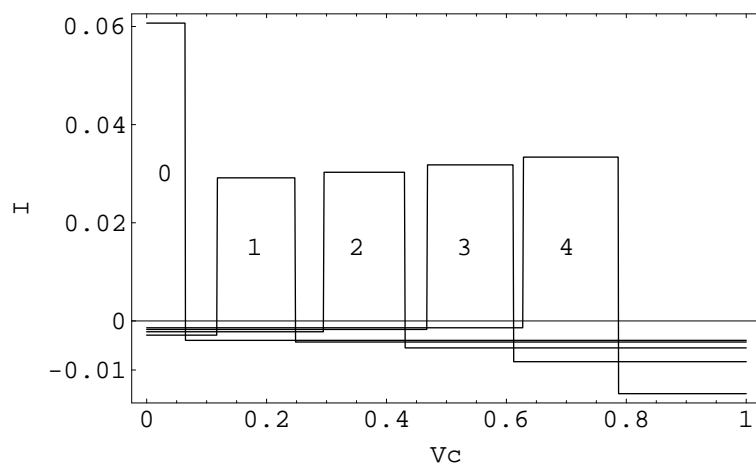


Fig.8